



RESEARCH ARTICLE

10.1002/2017GC007191

Key Points:

- Bedrock and detrital zircon (U-Th)/He thermochronometry provide evidence for exhumation of Lesser Himalayan strata enriched in ^{187}Os at ~16 Ma
- Seawater $^{187}\text{Os}/^{188}\text{Os}$ and $^{87}\text{Sr}/^{86}\text{Sr}$ trends at 16 Ma reflect shifts in Himalayan weathering substrates, which are influenced by the thrust belt kinematic evolution
- Shifts in weathering substrates can drive changes in seawater $^{187}\text{Os}/^{188}\text{Os}$ and $^{87}\text{Sr}/^{86}\text{Sr}$ records independent from changes in global weathering rates

Supporting Information:

- Supporting Information S1
- Data Set S1
- Data Set S2
- Data Set S3

Correspondence to:

C. Colleps,
ccolleps@hku.hk

Citation:

Colleps, C. L., Ryan McKenzie, N., Stockli, D. F., Hughes, N. C., Singh, B. P., Webb, A. A. G., . . . Horton, B. K. (2018). Zircon (U-Th)/He thermochronometric constraints on Himalayan thrust belt exhumation, bedrock weathering, and Cenozoic seawater chemistry. *Geochemistry, Geophysics, Geosystems*, 19, 257–271. <https://doi.org/10.1002/2017GC007191>

Received 17 AUG 2017

Accepted 1 JAN 2018

Accepted article online 8 JAN 2018

Published online 24 JAN 2018

Zircon (U-Th)/He Thermochronometric Constraints on Himalayan Thrust Belt Exhumation, Bedrock Weathering, and Cenozoic Seawater Chemistry

Cody L. Colleps^{1,2} , N. Ryan McKenzie^{2,3}, Daniel F. Stockli¹ , Nigel C. Hughes⁴, Birendra P. Singh⁵, A. Alexander G. Webb², Paul M. Myrow⁶, Noah J. Planavsky³, and Brian K. Horton^{1,7} 

¹Department of Geological Sciences, Jackson School of Geosciences, University of Texas at Austin, TX, USA, ²Department of Earth Sciences, University of Hong Kong, Pokfulam, Hong Kong, China, ³Department of Geology and Geophysics, Yale University, New Haven, CT, USA, ⁴Department of Earth Sciences, University of California, Riverside, CA, USA, ⁵Department of Geology, Panjab University, Chandigarh, Punjab, India, ⁶Department of Geology, Colorado College, Colorado Springs, CO, USA, ⁷Institute for Geophysics and Department of Geological Sciences, Jackson School of Geosciences, University of Texas at Austin, Austin, TX, USA

Abstract Shifts in global seawater $^{187}\text{Os}/^{188}\text{Os}$ and $^{87}\text{Sr}/^{86}\text{Sr}$ are often utilized as proxies to track global weathering processes responsible for CO_2 fluctuations in Earth history, particularly climatic cooling during the Cenozoic. It has been proposed, however, that these isotopic records instead reflect the weathering of chemically distinctive Himalayan lithologies exposed at the surface. We present new zircon (U-Th)/He thermochronometric and detrital zircon U-Pb geochronologic evidence from the Himalaya of northwest India to explore these contrasting interpretations concerning the driving mechanisms responsible for these seawater records. Our data demonstrate in-sequence southward thrust propagation with rapid exhumation of Lesser Himalayan strata enriched in labile ^{187}Os and relatively less in radiogenic ^{87}Sr at ~16 Ma, which directly corresponds with coeval shifts in seawater $^{187}\text{Os}/^{188}\text{Os}$ and $^{87}\text{Sr}/^{86}\text{Sr}$. Results presented here provide substantial evidence that the onset of exhumation of ^{187}Os -enriched Lesser Himalayan strata could have significantly impacted the marine $^{187}\text{Os}/^{188}\text{Os}$ record at 16 Ma. These results support the hypothesis that regional weathering of isotopically unique source rocks can drive seawater records independently from shifts in global-scale weathering rates, hindering the utility of these records as reliable proxies to track global weathering processes and climate in deep geologic time.

1. Introduction

Weathering processes play fundamental roles in regulating atmospheric CO_2 concentrations. The weathering of calcium-silicate minerals provides an important mechanism to draw down CO_2 , which helps to stabilize Earth's climate (Berner et al., 1983; Kump et al., 2000). Conversely, shifts in the extent of oxidative weathering of sulfides, which provides an alternative source of acidity to drive carbonate dissolution, may be a geologically significant source of atmospheric CO_2 (Torres et al., 2014). The important influence of chemical weathering on long-term carbon cycling motivates efforts to track the extent of global weathering processes through geologic time. Seawater strontium ($^{87}\text{Sr}/^{86}\text{Sr}_{(\text{sw})}$) and osmium ($^{187}\text{Os}/^{188}\text{Os}_{(\text{sw})}$) isotopic records, deciphered from well dated authigenic marine minerals and sediment (Hodell et al., 1991; Pegram et al., 1992; Ravizza, 1993; Veizer, 1989; Veizer et al., 1999), have emerged as two principal global weathering proxies (e.g., Misra & Froelich, 2012; Palmer & Edmond, 1989; Peucker-Ehrenbrink & Ravizza, 2000).

The isotopic composition of seawater Sr and Os represents a balance between oceanic hydrothermal fluxes and riverine input derived from subaerial chemical weathering of crustal rock. Mantle-derived hydrothermal input is depleted in radiogenic ^{87}Sr and ^{187}Os , whereas continental crust is isotopically enriched in these isotopes due to the decay of ^{87}Rb and ^{187}Re , respectively. Therefore, increases in global continental silicate weathering may generate increases in $^{87}\text{Sr}/^{86}\text{Sr}_{(\text{sw})}$ and $^{187}\text{Os}/^{188}\text{Os}_{(\text{sw})}$. Various crustal rocks contain appreciable amounts of radiogenic ^{87}Sr that can be supplied to the ocean from weathering, albeit the weathering efficiency of different rock types can influence the relative contributions of Sr from a given region (Bickle

et al., 2001, 2015; Edmond, 1992; Harris, 1995; Quade et al., 2003). Organic-rich black shale is markedly enriched in labile Os and dominates the riverine flux (Pegram et al., 1992; Peucker-Ehrenbrink & Ravizza, 2000). Extraterrestrial sources also contribute background non-radiogenic Os to the oceans (Peucker-Ehrenbrink & Ravizza, 2000). Consequently, marine Os isotope records are thought to track the global weathering of Os-bearing lithologies with ^{187}Os being primarily sourced from organic-rich sediments, likely linked to sulfide oxidation (e.g., Georg et al., 2013; Torres et al., 2014), whereas Sr isotopes are assumed to track either overall silicate weathering (e.g., Raymo & Ruddiman, 1992) or variation in weathering of endmember mafic and silicic bedrock (e.g., Bataille et al., 2017; Cox et al., 2016; Godd ris et al., 2017). Isotopic compositions of crustal rocks are highly influenced by their age, lithology, and degree of alteration, and these parameters account for the diverse spatial distribution of bedrock $^{87}\text{Sr}/^{86}\text{Sr}$ and $^{187}\text{Os}/^{188}\text{Os}$ values. Given this non-homogeneous spatial and stratigraphic distribution of crustal rocks enriched in particular isotopes, as well as a spatiotemporal variance in tectonic unroofing, it is unlikely that these seawater records are driven solely by increases and decreases in silicate weathering rates.

A marked increase in seawater $^{87}\text{Sr}/^{86}\text{Sr}$ during the Cenozoic is often assumed to reflect increased silicate weathering associated with the Himalayan–Tibetan orogeny, and this increase is considered to be a primary mechanism to drive Cenozoic global cooling (e.g., Raymo & Ruddiman, 1992; Sarin et al., 1989). Indeed, the Himalayan system is a zone characterized by high chemical weathering rates, which are due to the hot and humid conditions of the South Asian monsoon (West et al., 2002). However, numerous studies have demonstrated that elevated $^{87}\text{Sr}/^{86}\text{Sr}$ in Himalayan rivers is not always correlative to high dissolution rates of silicate rocks, but rather to compositional differences in bedrock being weathered, thus questioning the utility of seawater $^{87}\text{Sr}/^{86}\text{Sr}$ (Blum et al., 1998; English et al., 2000; Galy et al., 1999; Harris et al., 1998; Quade et al., 1997, 2003). The utility of the $^{87}\text{Sr}/^{86}\text{Sr}_{(\text{sw})}$ record to model the deep time carbon cycle may, thus, overestimate CO_2 consumption due to silicate weathering (Blum et al., 1998). More recently, the exhumation of bedrock enriched in ^{187}Os presently preserved in the Lesser Himalayan zone of northwest India (Figures 1 and 2) has been proposed to drive the abrupt increase in $^{187}\text{Os}/^{188}\text{Os}_{(\text{sw})}$ at ~ 16 Ma (Myrow et al., 2015). To further explore the relationship between regional source rock weathering and observed shifts in Cenozoic seawater chemistry, we focus on the Himalaya of northwest India and attempt to use *in situ* and detrital low temperature zircon (U-Th)/He (ZHe) thermochronometric data to directly constrain the timing of exhumation of isotopically enriched Lesser Himalayan bedrock.

2. Geologic Background

2.1. Lesser Himalaya of Northwest India

The Himalayan thrust belt consists of distinct fault-bounded tectonostratigraphic zones that span the entire orogeny (Yin, 2006). These are, from south to north, the Sub Himalaya (SH), Lesser Himalaya (LH), and Main Central Thrust (MCT) hanging wall that includes the Greater Himalayan sequence (GH) and Tethyan Himalaya (TH) (Figure 1). The LH resides structurally in the footwall of the MCT and is juxtaposed against Cenozoic SH foreland basin deposits to the south by the Main Boundary Thrust (MBT) system. In northwest India, the now folded Tons thrust separates the LH into the outer LH (oLH), which consists of low-grade Neoproterozoic to Cambrian metasedimentary rocks, and the inner LH (iLH), which consists of late Paleoproterozoic to Mesoproterozoic metasedimentary rocks and gneisses (Ahmad et al., 2000; Celerier et al., 2009b; Hughes et al., 2005; Jiang et al., 2002; McKenzie et al., 2011; Richards et al., 2005; Valdiya, 1980; Webb et al., 2011). Lower-grade iLH rocks of the Tons thrust footwall, including those of the Berinag Group, generally exhibit greenschist facies metamorphism with peak metamorphic temperatures ranging from $<330^\circ\text{C}$ to 390°C (Celerier et al., 2009a). Higher-grade garnet-, kyanite-, and sillimanite-bearing iLH rocks of the Munsiri Group underwent Late Miocene prograde metamorphism with peak temperatures between ~ 600 and 700°C (Caddick et al., 2007; Chambers et al., 2009; Vannay et al., 2004). Numerous MCT hanging-wall klippen of highly variable metamorphic grades (i.e., upper greenschist facies rocks and mylonitic augen gneisses) are preserved above LH rocks. South of the Tons thrust, these klippen are structurally emplaced above lower greenschist facies oLH rocks that record peak metamorphic temperatures not exceeding $\sim 330^\circ\text{C}$ (Celerier et al., 2009a). Whereas iLH strata have correlative, age-equivalent strata along strike across the Himalaya, exposure and preservation of oLH strata is mostly limited to northwest India where these rocks are preserved within structural synforms (Auden, 1934; Celerier et al., 2009b; Hughes, 2016; Valdiya, 1980; Webb et al., 2011). While the precollisional origin of oLH rocks has been debated, it is certain that Cambrian

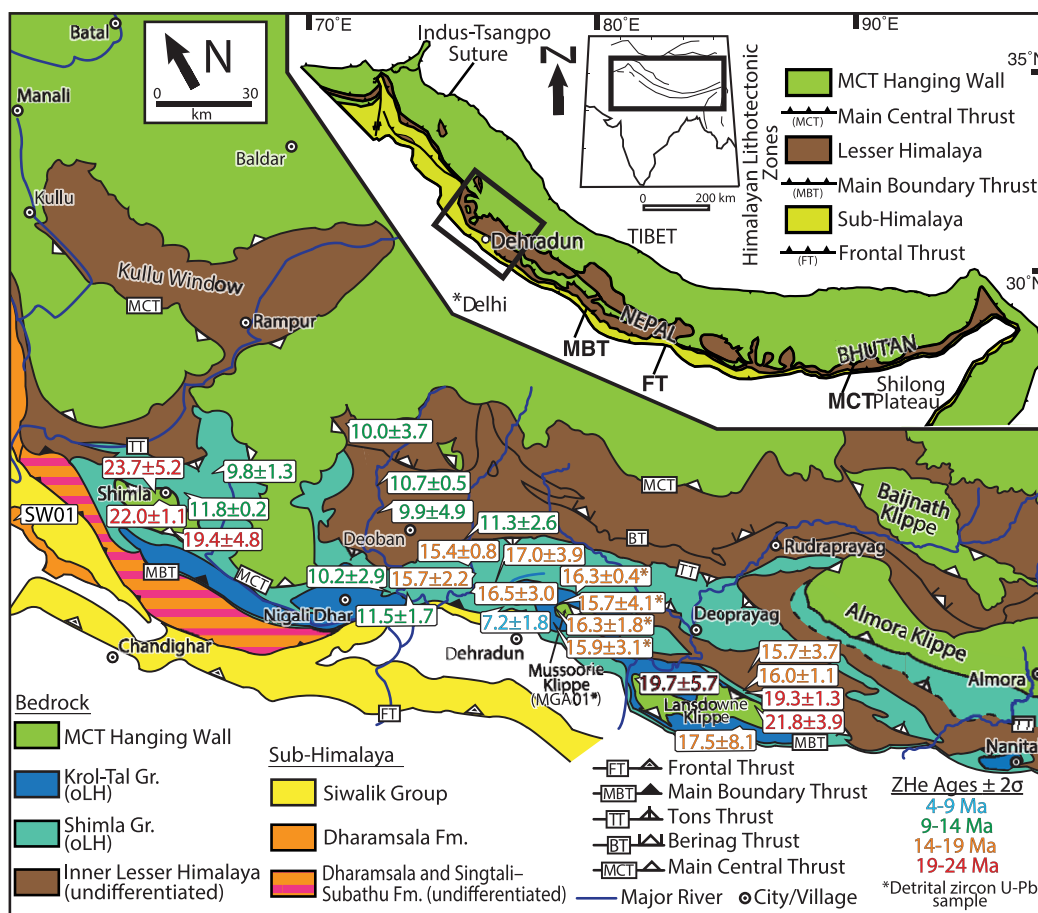


Figure 1. Simplified geologic map of the northwest Indian Himalaya with ZHe ages. Zircon (U-Th)/He ages from multiple grains analyzed from each locality are plotted as mean ages with an error of 2σ (data reported in supporting information). The location of foreland basin sample analyzed for detrital ZHe ages is marked by sample name SW01. Map modified after Celerier et al. (2009b), Myrow et al. (2015), Valdiya (1980), and Yu et al. (2015).

sedimentation extended far onto the Indian craton, and likely that oLH rocks were deposited along a continuous Indian margin as part of an extensive sedimentary belt that spanned from Pakistan to the eastern syntaxis, and south onto the craton (Hughes, 2016; McKenzie et al., 2011; Myrow et al., 2003, 2015). Along-strike variations in the structural geometry of the Tons thrust have demonstrated how oLH strata, currently preserved in northwest India, have likely been eroded away in Nepal (Yu et al., 2015) where Paleoproterozoic LH rocks are widely exposed as structurally repeated units within the LH duplex (DeCelles et al., 2001; Robinson & Martin, 2014; Robinson et al., 2003).

The Mussoorie syncline of northwest India preserves one of the most complete stratigraphic records of oLH rocks and includes, from base to top: mixed siliciclastic rocks of the Shimla Group, the diamictite-bearing Blaini Formation, Krol Group carbonate, and fossiliferous mixed siliciclastic strata of the Tal Group (Figure 3) (Hughes et al., 2005; Jiang et al., 2002; Singh et al., 1999; Valdiya, 1980). Near Mussoorie and Lansdowne, shallow marine deposits of the Cretaceous to Paleogene Subathu–Singtali Formations unconformably overlie the Tal Group, where they are preserved structurally below higher grade MCT hanging wall klippen. To the west, the Shimla MCT klippe is structurally emplaced directly atop the oLH Shimla Group rocks. Nanital marks the easternmost known extent of exposed oLH Krol–Tal Group rocks (Figure 1). Preservation of the Krol–Tal belt of the upper oLH in northwest India is particularly significant as it contains black shale units enriched in radiogenic ¹⁸⁷Os (Figures 2 and 3) (Singh et al., 1999). The exhumation and weathering of these shale deposits are proposed to be the initial contributors to the ~16 Ma Neogene increase in ¹⁸⁷Os/¹⁸⁸Os_(sw) (Myrow et al., 2015).

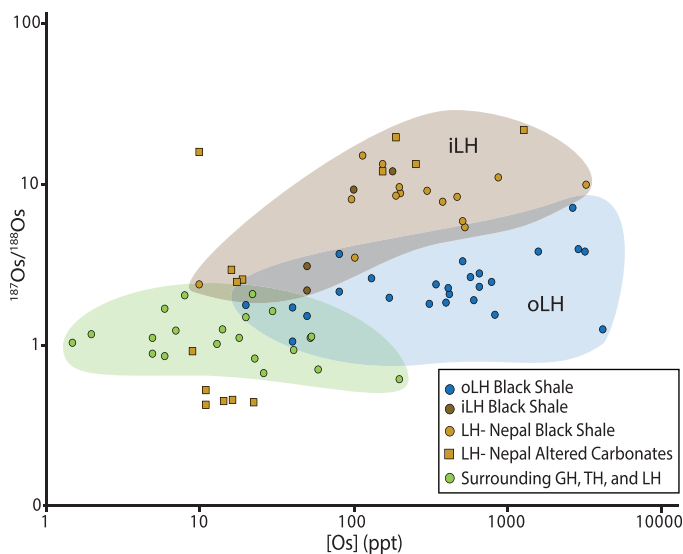


Figure 2. Compilation of Himalayan bedrock $^{187}\text{Os}/^{188}\text{Os}$ values and Os concentrations from various tectonostratigraphic units and lithologies. Distinct $^{187}\text{Os}/^{188}\text{Os}$ values and Os concentrations are present for oLH black shales highlighted in blue, Paleoproterozoic LH black shale and altered carbonate highlighted in brown, and surrounding GH, TH, and LH rocks of differing lithologies (not black shale) highlighted in green. LH black shale is distinctively enriched in $^{187}\text{Os}/^{188}\text{Os}$ in high concentrations compared to surrounding rocks. Data compiled from Singh et al. (1999) and Pierson-Wickmann et al. (2000, 2002) (see supporting information for compiled data).

2.2. Himalayan Orogenesis and Cenozoic Seawater Chemistry

Isotopic compositions of Himalayan rocks vary substantially between different tectonostratigraphic zones and rock types across the orogen. Lesser Himalayan black shale units, for example, are markedly enriched with high concentrations of radiogenic Os and yield anomalously high $^{187}\text{Os}/^{188}\text{Os}$ values ranging from +2 to exceptionally high values of +14 compared to surrounding rocks of the GH and TH, with typical bedrock values ranging from ~ 0.5 – 1.5 (Figure 2) (Pierson-Wickmann et al., 2000; Singh et al., 1999). Isotopically enriched black shale and enriched fine-grained clastic rocks occur as centimeter to tens of meters thick beds, which are persistent throughout oLH sequences (Figure 3) and low-grade metasedimentary rocks of the iLH. Impure Precambrian marbles within the LH of Nepal are also enriched in $^{187}\text{Os}/^{188}\text{Os}$ (Figure 2) (Pierson-Wickmann et al., 2002). Considering their organic carbon-poor protoliths, the radiogenic Os component in these marbles was likely provided by hydrothermal interaction with altered radiogenic black shale (Pierson-Wickmann et al., 2002). Carbonates within the oLH Krol Group are relatively less enriched in radiogenic Sr with $^{87}\text{Sr}/^{86}\text{Sr}$ values of 0.709 to 0.714 (Singh et al., 1998) compared to GH rocks of the MCT hanging wall, with typical $^{87}\text{Sr}/^{86}\text{Sr}$ values of 0.74–0.78 (France-Lanord et al., 1993). Paleoproterozoic LH strata, however, are highly enriched in radiogenic Sr with $^{87}\text{Sr}/^{86}\text{Sr}$ values of 0.8–1.0, consistent with their long crustal evolution (Bickle et al., 2001; France-Lanord et al., 1993).

In northwest India, the MCT has been mapped as two distinct strands, MCT-I and MCT-II, and the immediate hanging wall rocks of

these strands are divided into the Vaikrita and Muniari groups, respectively (Ahmad et al., 2000; Celerier et al., 2009a, 2009b; Richards et al., 2005; Valdiya, 1980). Vaikrita Group rocks yield similar $^{87}\text{Sr}/^{86}\text{Sr}$ values comparable to those from MCT hanging wall rocks elsewhere in the orogen. The high-grade rocks of the Muniari Group formed from protoliths similar in age to Paleoproterozoic iLH rocks (Mandal et al., 2015, 2016; Robinson & Pearson, 2013), and thus yield similar isotopic compositions to iLH and LH rocks of Nepal—in fact, Muniari rocks have yielded some of the highest $^{87}\text{Sr}/^{86}\text{Sr}$ ratios in the Himalayan orogen (e.g., >1.04) (Ahmad et al., 2000; Bickle et al., 2001). In northwest India, crystalline rocks from the Askot klippe are composed of Paleoproterozoic rocks of Muniari affinity (Mandal et al., 2016), while rocks from the Almora klippe show GH affinity (Mandal et al., 2015). Coupled with structural constraints (Webb et al., 2011; Yu et al., 2015), these relationships suggest that MCT hanging wall klippen south of the Almora klippe, including the Lansdowne and Mussoorie klippen, are likely to be of GH or TH affinity, and thus yield comparable $^{87}\text{Sr}/^{86}\text{Sr}$ values.

The continuous rise in $^{87}\text{Sr}/^{86}\text{Sr}_{(\text{sw})}$ that initiated at ~ 35 Ma, as well as shifts observed in Neogene $^{187}\text{Os}/^{188}\text{Os}_{(\text{sw})}$, have long been attributed to weathering associated with Cenozoic Himalayan–Tibetan uplift, although it remains unclear whether this reflects an overall increase in the extent of silicate weathering (Raymo & Ruddiman, 1992) or the exhumation and weathering of markedly radiogenic bedrock (Blum et al., 1998; Edmond, 1992; Myrow et al., 2015; Quade et al., 1997). Following a ~ 15 Myr period of relative stasis, a notable increase in $^{187}\text{Os}/^{188}\text{Os}_{(\text{sw})}$ initiated at 16 Ma with a coeval decrease in the rate of increase of $^{87}\text{Sr}/^{86}\text{Sr}_{(\text{sw})}$ (Figure 4a). This initial increase in $^{187}\text{Os}/^{188}\text{Os}_{(\text{sw})}$ was originally attributed to Himalayan uplift based on broad temporal coincidence (Pegram et al., 1992), and was later linked to exhumation of ^{187}Os -enriched LH black shale (Pierson-Wickmann et al., 2000; Singh et al., 1999). Presumed timing constraints on the exhumation of ^{187}Os enriched LH rocks at ~ 11 Ma from Nepal impeded this correlation (Chesley et al., 2000), but these constraints do not account for exhumation of ^{187}Os enriched strata from the oLH presently preserved in northwest India.

Recent advances in reconstructing the kinematic evolution and stratigraphic architecture of the northwest Indian Himalaya, however, support earlier exhumation of ^{187}Os enriched, black-shale-bearing LH strata at ~ 16 Ma. Revised kinematic models (e.g., Webb, 2013; Webb et al., 2011; Yu et al., 2015), coupled with mass-balance modeling that showed a profound Os contribution from a discrete oLH black shale unit, prompted

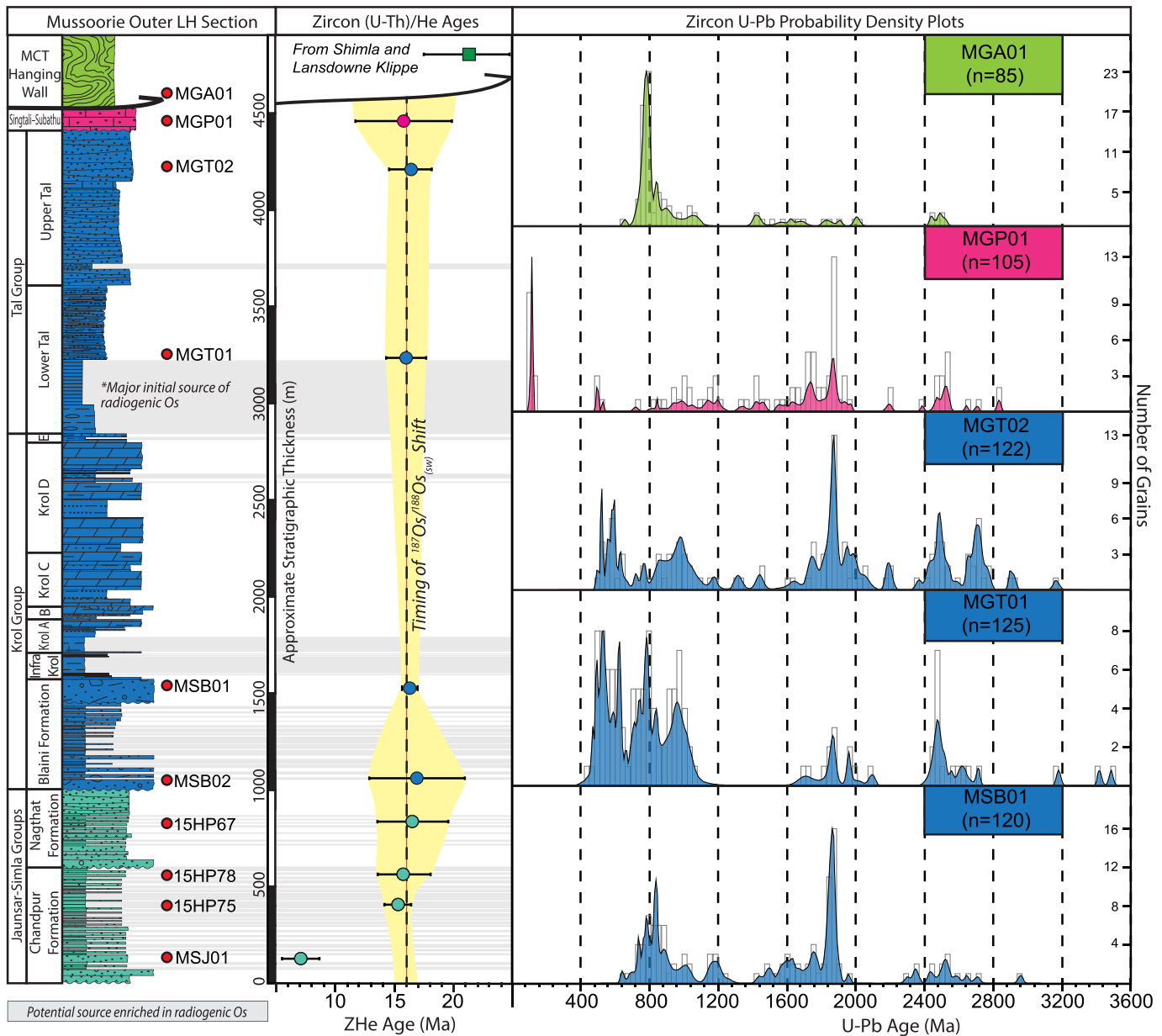


Figure 3. Simplified stratigraphic section of the oLH preserved within the Mussoorie syncline with bedrock U-Pb and (U-Th)/He results. The stratigraphic position of samples collected for analyses are marked on an idealized stratigraphic section of the oLH in Mussoorie, which shows variation in grain size and lithology. Grey bars represent potential fine-grained sources enriched in radiogenic Os, and a prominent unit from the oLH is noted as the proposed black shale source responsible for the initial increase in seawater $^{187}\text{Os}/^{188}\text{Os}$. Zircon (U-Th)/He ages show a uniform ~ 16 Ma age throughout $\sim 3\text{--}4$ km of section from the lower oLH Shimla Group to the Singtali–Subathu Formations, which lies unconformably above the upper Tal Group. NOTE: The Jaunsar-Simla Group thickness represents a minimum thickness, and the unit may exceed a thickness of ~ 3 km (Jiang et al., 2003).

the proposal that the rapid increase in $^{187}\text{Os}/^{188}\text{Os}_{(\text{sw})}$ and coeval reduced slope in $^{87}\text{Sr}/^{86}\text{Sr}_{(\text{sw})}$ at ~ 16 Ma (Figure 4a) resulted from a southward thrust advance and shift in exhumation away from MCT hanging wall rocks to low-grade metasedimentary rocks of the oLH (Myrow et al., 2015). An additional relative increased rate in $^{87}\text{Sr}/^{86}\text{Sr}_{(\text{sw})}$ was initiated at ~ 8 Ma following a period when Himalayan Sr flux decreased from its peak at ~ 16 Ma (Derry & France-Lanord, 1996). Importantly, mass-balance models demonstrate that the Neogene seawater record can be largely explained by compositional changes in the material being weathered in different Himalayan thrust sheets without any change in global silicate weathering (Myrow et al., 2015).

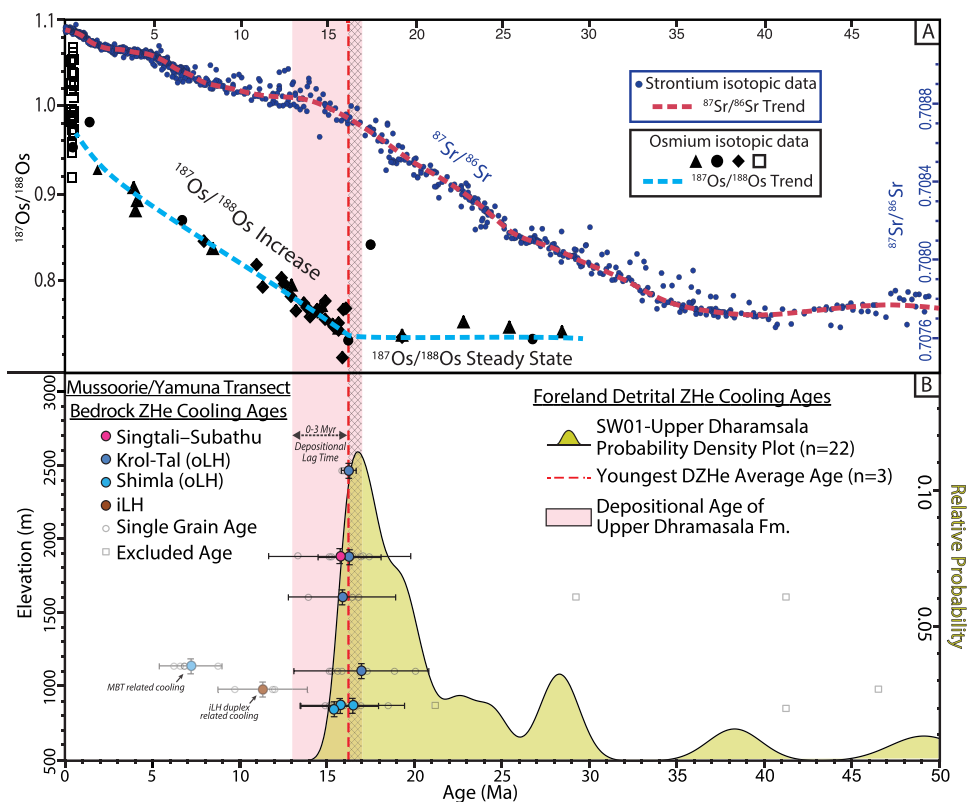


Figure 4. (a) Global $^{187}\text{Os}/^{188}\text{Os}$ and $^{87}\text{Sr}/^{86}\text{Sr}$ Neogene seawater records with (b) Himalayan ZHe ages. The pink bar represents the depositional age range of the upper Dharamsala Formation. Detrital ZHe results from sample SW01 are represented by the yellow probability density plot. Bedrock ZHe average ages from the Mussoorie region, as well as single aliquot ages from each sample, are plotted in relation to their elevation, and show uniform ~ 16 Ma cooling ages from the oLH collected across ~ 1.5 km of topographic relief. Two samples with notably younger ages are the result of different cooling events. See text for detailed explanations. Seawater records from compilations of Myrow et al. (2015) and Misra and Froelich (2012).

The hypothesized 16 Ma LH exhumation was primarily based on constraints derived from regional foreland basin records (e.g., Najman et al., 2009; White et al., 2002), with additional support provided by evidence for LH deformation prior to 11 Ma in regions further along strike (e.g., Long et al., 2012). Foreland provenance shifts at ~ 16 Ma are recorded by an overall upward coarsening of clastic deposits, a decreased contribution of metamorphic detritus, and a marked increase in depositional lag time—the temporal difference between the mineral cooling age during exhumation and the depositional age in the basin (Reiners & Brandon, 2006; Ruiz et al., 2004)—of detrital white mica $^{40}\text{Ar}/^{39}\text{Ar}$ ages that represent a shift from high-grade GH rocks to low-grade LH rocks that lack Cenozoic age white mica (Najman et al., 2009; White et al., 2002). While these data clearly demonstrate the likelihood of earlier exhumation of LH rocks than that generally presumed (Chesley et al., 2000), the initial timing of LH exhumation continues to be widely disputed within the community, likely stemming from conflicting models of the north Indian margin before the onset of Himalayan orogenesis (e.g., DeCelles et al., 2000, 2016; Hughes, 2016; Myrow et al., 2003, 2015). Despite its importance, the timing of onset of oLH exhumation has remained poorly constrained as these rocks have not, until now, been a focus for thermochronometric investigation. Here we provide new coupled thermochronometric and geochronologic constraints on the exhumation of the frontal Himalayan system of northwest India where a rich diversity of LH strata is widely exposed.

3. Methods

3.1. Zircon (U-Th)/He Thermochronometry

Low-temperature zircon (U-Th)/He (ZHe) thermochronometry has emerged as a valued geologic tool utilized to track the thermal evolution and exhumation of rocks in a variety of tectonic settings. This method is

Table 1
Bedrock Zircon (U-Th)/He Results and Sample Details

| Sample | Zone | Location | Formation/ lithology | Latitude | Longitude | Elevation (m) | Average Zhe Age (Ma) | 2SD | 2SE |
|---------------|------|------------------|-------------------------|----------------|----------------|------------------|-------------------------|------|------|
| STJ01 | MCT | Rampur | Haimanta | 31° 6'11.94"N | 77° 7'5.28"E | 1,025 | 23.70 | 5.20 | 1.73 |
| STJ02 | MCT | Rampur | Haimanta | 31° 5'43.74"N | 77° 8'17.70"E | 1,975 | 22.03 | 1.10 | 0.37 |
| 15HP01 | MCT | Rampur | Haimanta | 31° 1'16.64"N | 77° 6'6.00"E | 1,691 | 19.39 | 4.90 | 1.60 |
| 15UK12 | MCT | Lansdowne | MCT Quartzite | 30° 3'32.03"N | 78° 21'11.67"E | 850 | 19.71 | 5.73 | 1.91 |
| 15UK25 | MCT | Lansdowne | MCT Gneiss | 29° 51'26.80"N | 78° 40'43.60"E | 1,610 | 21.80 | 3.90 | 1.30 |
| 15HP70 | iLH | Mussoorie/Yamuna | Damtha | 30° 38'57.57"N | 78° 1'25.25"E | 967 | 11.31 | 2.57 | 0.86 |
| TV-17-RT-DB22 | iLH | Tons | Rautgara | 30° 54'35.94"N | 77° 49'56.94"E | 825 | 10.68 | 0.47 | 0.12 |
| TV-17-RTG-1 | iLH | Tons | Rautgara | 30° 50'0.18"N | 77° 46'40.14"E | 837 | 9.88 | 4.87 | 0.81 |
| TVP-BNG-18 | iLH | Tons | Berinag | 31° 7'34.50"N | 77° 49'48.06"E | 1,178 | 9.98 | 3.68 | 0.74 |
| 15UK16 | iLH | Lansdowne | Damtha? | 29° 57'18.42"N | 78° 45'39.06"E | 680 | 15.67 | 3.72 | 0.93 |
| MGP01 | oLH | Mussoorie/Yamuna | Subathu–Singtali | 30° 22'0.00"N | 78° 12'56.64"E | 1,859 | 15.73 | 4.08 | 1.36 |
| MGT01 | oLH | Mussoorie/Yamuna | Tal | 30° 20'57.90"N | 78° 10'51.30"E | 1,583 | 15.87 | 3.08 | 1.03 |
| MGT02 | oLH | Mussoorie/Yamuna | Tal | 30° 22'7.20"N | 78° 12'55.62"E | 1,851 | 16.30 | 1.81 | 0.30 |
| MSB01 | oLH | Mussoorie/Yamuna | Blaini | 30° 24'52.50"N | 78° 16'17.40"E | 2,429 | 16.25 | 0.42 | 0.11 |
| MSB02 | oLH | Mussoorie/Yamuna | Blaini | 30° 30'29.94"N | 77° 59'58.92"E | 1,090 | 16.98 | 3.87 | 0.55 |
| TV-BLD | oLH | Tons | Blaini | 30° 35'43.38"N | 77° 44'44.40"E | 612 | 10.15 | 2.89 | 1.45 |
| TV-J | oLH | Tons | Nagthat | 30° 34'34.38"N | 77° 45'51.06"E | 616 | 11.53 | 1.69 | 0.56 |
| STJ03 | oLH | Rampur | Shimla | 31° 6'21.06"N | 77° 11'36.96"E | 2,176 | 11.82 | 0.23 | 0.11 |
| STJ04 | oLH | Rampur | Shimla | 31° 5'12.18"N | 77° 17'46.20"E | 2,517 | 9.81 | 1.29 | 0.43 |
| MSJ01 | oLH | Mussoorie/Yamuna | Shimla | 30° 24'57.66"N | 78° 4'39.60"E | 1,122 | 7.18 | 0.90 | 0.15 |
| 15UK19 | oLH | Lansdowne | Shimla | 29° 54'51.90"N | 78° 42'27.20"E | 706 | 19.26 | 1.35 | 0.45 |
| 15UK22 | oLH | Lansdowne | Tal | 29° 54'26.97"N | 78° 41'45.67"E | 984 | 16.00 | 1.13 | 0.56 |
| 15UK29 | oLH | Lansdowne | Tal | 29° 49'6.28"N | 78° 37'0.88"E | 752 | 17.51 | 8.18 | 2.73 |
| 15HP67 | oLH | Mussoorie/Yamuna | Nagthat | 30° 31'9.00"N | 77° 57'35.88"E | 858 | 16.46 | 3.00 | 0.75 |
| 15HP68 | oLH | Mussoorie/Yamuna | Shimla | 30° 32'44.07"N | 77° 59'6.54"E | 857 | 15.73 | 2.23 | 0.56 |
| 15HP75 | oLH | Mussoorie/Yamuna | Shimla | 30° 34'2.33"N | 78° 0'19.51"E | 835 | 15.41 | 0.08 | 0.02 |

based on the thermally activated diffusion of radiogenic ⁴He—an alpha (α) particle produced during the radioactive decay of ²³⁸U, ²³⁵U, ²³²Th and ¹⁴⁷Sm—out of a given crystal lattice. The ZHe system is characterized by a ⁴He closure temperature (T_c) of ~180°C, corresponding to exhumation from depths of ~7 to ~9 km and a partial retention zone (PRZ) between ~140 and 200°C (Reiners & Brandon, 2006; Reiners et al., 2004). In the Himalayan fold-and-thrust belt, where rapid exhumation is common (Deeken et al., 2011; Long et al., 2012; Thiede et al., 2004), it can be assumed that rocks at the surface rapidly passed through the ZHe PRZ and that the time spent in the PRZ is negligible. Rocks that are sufficiently buried to reset the ZHe system and rapidly cooled through the PRZ are also unlikely to exhibit the effects of radiation damage on the ZHe system (Guenther et al., 2013), such that ZHe age dispersion within a single sample should be minimal, and the average age of single grain ages from each sample should adequately represent the time that the rock passed through the ZHe PRZ. For these reasons, ZHe ages presented here are assumed to represent the time that rocks were exhumed through the ZHe T_c of ~180°C.

In order to constrain the timing of LH exhumation, we collected new ZHe ages from 26 bedrock samples collected along strike-perpendicular transects across major tectonostratigraphic zones of the frontal thrust belt (Figure 1 and Table 1). Sampling focused largely on the diverse iLH strata north of the Tons thrust, near complete oLH stratigraphic sections south of the Tons thrust, and MCT hanging wall klippen which structurally overlie oLH rocks near the front of the thrust system. One foreland basin sample (SW01), collected from the ~13–17 Ma Upper Dharamsala Formation exposed in the SH near the Sutlej River, was also analyzed for detrital ZHe ages. The coupling of bedrock and detrital ZHe data provides direct, quantitative constraints on the timing of Himalayan cooling and exhumation during progressive thrusting, erosion, and deposition of erosional products shed into the foreland basin.

For each bedrock sample, 4–7 zircon crystals were handpicked for ZHe ages, and the average age of multiple grain aliquots for each sample are reported with an error of 2 standard deviations (2SD). For detrital ZHe analysis on sample SW01, 22 zircon crystals were selected for ZHe ages. Ages younger than 55 Ma were

plotted as a probability density plot, and the youngest three ZHe ages were averaged to constrain a maximum depositional age of the sample. All ZHe data were collected at the UTChron facilities at the University of Texas at Austin following analytical procedures of Wolfe and Stockli (2010). All ZHe data with complete methodology can be found in the supporting information (Dodson, 1973; Farley et al., 1996; Reiners et al., 2002, 2004; Zeitler et al., 1987).

3.2. Detrital Zircon U-Pb Geochronology

Detrital zircon U-Pb geochronology has developed into a powerful geologic tool often utilized to fingerprint potential provenance sources and to help define and distinguish distinct tectonostratigraphic boundaries in complex tectonic settings (DeCelles et al., 2000; Mandal et al., 2015, 2016; McKenzie et al., 2011; McQuarrie et al., 2008; Myrow et al., 2003, 2010; Webb et al., 2011). In order to put stratigraphic and structural constraints on bedrock samples collected for ZHe cooling ages, we analyzed 5 samples for detrital zircon U-Pb ages collected from the Mussoorie syncline (Figure 3), which preserves one of the most complete records of the oLH, with MCT hanging wall rocks emplaced structurally above the oLH referred to as the Mussoorie klippe. For each sample, at least 120 zircons were analyzed for U-Pb ages via laser ablation ICP-MS, and grains with greater than 10% discordance were rejected. Detrital zircon U-Pb age results were plotted as probability density plots and histograms with a bin width of 30 Myrs for each sample. All U-Pb analyzes were performed at the University of Texas at Austin UTChron facilities via laser ablation ICP-MS (Feng et al., 1993; Fryer et al., 1993). Detrital zircon U-Pb data and complete methodology can be found in the supporting information (Paton et al., 2011; Petrus & Kamber, 2012; Vermeesch, 2004).

4. Results

4.1. Zircon (U-Th)/He Thermochronometry

To the west of Mussoorie, near Shimla, four samples from the lower oLH Shimla Group yielded ZHe ages between ~10 and 12 Ma, with an average age of 10.7 ± 2.4 Ma ($n = 11$). Three samples analyzed from the Shimla MCT klippe, which structurally overlies the Shimla Group strata, yielded ZHe ages between ~19.5 and 24.0 Ma, with an average age of 21.9 ± 5.3 Ma ($n = 10$). To the east of Mussoorie near Lansdowne, four LH samples ranging stratigraphically from the upper iLH to the oLH upper Tal Group yielded ages ranging from 15.7 ± 3.7 to 19.3 ± 1.4 Ma with an average age of 17.1 ± 5.2 Ma ($n = 12$). Two samples, one gneiss and one quartzite, collected from the Lansdowne MCT klippe yielded ages of 21.8 ± 3.9 Ma and 19.7 ± 5.7 Ma respectively, with a compiled average age of 20.6 ± 5.0 Ma ($n = 5$).

Nine oLH samples were collected within the Mussoorie syncline and provide data from the most complete stratigraphic oLH successions that we studied (Figure 3). Three samples from the stratigraphically lower Shimla Group yielded ages ranging from 15.4 ± 0.1 Ma to 16.5 ± 3.0 Ma with an average ZHe cooling age of 16.0 ± 2.3 Ma ($n = 9$). Four bedrock samples from the Krol–Tal belt of the upper oLH yielded an average cooling age of 16.5 ± 2.7 Ma ($n = 20$), and one sample from the Cretaceous–Paleogene Singtali–Subathu Formations, which rests unconformably on these rocks, yielded an age of 15.7 ± 4.1 Ma ($n = 3$). Samples analyzed from the Krol–Tal belt include those from the Marinoan-aged Blaini diamictite, collected below the cap carbonate that marks the base of the ~1.5 km thick Krol Group (Jiang et al., 2002), and sandstone from the biostratigraphically constrained Cambrian Tal Group that overlies the Krol Group (Hughes et al., 2005). These samples were collected on both the northern and southern limbs of the Mussoorie syncline (Figure 1). The Singtali–Subathu sample was deposited onto the Tal Group before LH deformation and caps the entire 2–3 km thick Blaini–Krol–Tal package. A single lower oLH Shimla Group sample collected just north of the MBT, and south of the Mussoorie MCT klippe, produced an age of 7.2 ± 1.8 Ma ($n = 6$), marking the youngest ZHe cooling age presented here. Samples collected from the Mussoorie MCT klippe yielded zircons that were too small for ZHe analyzes. Four samples analyzed from the iLH north of the Tons thrust, along the Tons and Yamuna rivers, yielded ZHe ages ranging from ~10.0–11.5 Ma, with a compiled average of 10.3 ± 3.5 Ma ($n = 18$).

Detrital ZHe analysis on 22 zircon grains from a foreland basin sample (SW01) of the 13–17 Ma upper Dharmsala Formation exhibit a predominant relative probability age peak of ~17 Ma, and a smaller age group of 20–30 Ma (Figure 4b and Table 2). Six detrital grains yielded ZHe ages older than 50 Ma and were likely sourced or recycled from bedrock not thermally reset by Himalayan orogenesis. The youngest three detrital grains produced an average ZHe age of 16.2 ± 0.5 Ma ($n = 3$), which marks a maximum depositional age for

Table 2
Detrital Zircon (U-Th)/He Results and Sample Details

| Sample | Formation | Latitude | Longitude | Elevation (m) | Aliquot | Age, Ma | err., Ma |
|--------|------------------|---------------|---------------|---------------|-----------|---------|----------|
| | | | | | zSW01-48 | 15.99 | 1.28 |
| | | | | | zSW01-35 | 16.18 | 1.29 |
| | | | | | zSW01-53 | 16.51 | 1.32 |
| | | | | | zSW01-97 | 17.11 | 1.37 |
| | | | | | zSW01-18 | 17.26 | 1.38 |
| | | | | | zSW01-8 | 17.72 | 1.42 |
| | | | | | zSW01-49 | 18.37 | 1.47 |
| | | | | | zSW01-93 | 19.25 | 1.54 |
| | | | | | zSW01-1 | 19.40 | 1.55 |
| | | | | | zSW01-63 | 20.50 | 1.64 |
| SW01 | Upper Dharamsala | 31°12'41.52"N | 76°38'51.36"E | 461 | zSW01-19 | 22.44 | 1.80 |
| | | | | | zSW01-105 | 24.39 | 1.95 |
| | | | | | zSW01-44 | 28.29 | 2.26 |
| | | | | | zSW01-117 | 28.30 | 2.26 |
| | | | | | zSW01-111 | 38.33 | 3.07 |
| | | | | | zSW01-115 | 49.18 | 3.93 |
| | | | | | zSW01-108 | 62.23 | 4.98 |
| | | | | | zSW01-101 | 70.59 | 5.65 |
| | | | | | zSW01-76 | 147.89 | 11.83 |
| | | | | | zSW01-31 | 304.29 | 24.34 |
| | | | | | zSW01-71 | 316.80 | 25.34 |
| | | | | | zSW01-73 | 361.80 | 28.94 |

Note. Average age of three youngest dZHe grains: 16.22 ± 0.52 .

sample SW01. This further constrains the depositional age to ~ 16 – 13 Ma, and a depositional lag time of ~ 0 – 3 Myr.

4.2. Detrital Zircon U-Pb Geochronology

One sample from the Blaini diamictite (MSB01) yielded zircon U-Pb ages ranging from ~ 650 to $3,000$ Ma, which includes two major peaks at ~ 800 Ma and $\sim 1,800$ Ma. Two samples from the Tal Group (MGT01 and MGT02) both yielded ages ranging from ~ 450 to $3,500$ Ma, with prominent age clusters at ~ 450 – $1,050$ Ma, $1,800$ Ma, and $2,500$ – $2,800$ Ma. The youngest grains from these samples yielded rather large errors that overlap with the 485 Ma Cambrian-Ordovician boundary, so these results cannot reliably contest the biostratigraphically constrained Cambrian age of the Tal Group (Hughes et al., 2005). A sample from Singtali-Subathu deposits (MGP01), collected directly above sample MGT02, was also analyzed for detrital zircon analysis. While the age distribution between ~ 450 and $3,500$ Ma from sample MGP01 is similar to signatures of oLH rocks, with a large age peak at $1,800$ Ma, this sample also contains much younger, Early Cretaceous zircons with U-Pb ages of ~ 105 – 125 Ma. A sample collected from the Mussoorie MCT klippe (MGA01), structurally above sample MGP01, lacks any young Cretaceous grains, and yielded an age distribution ranging from ~ 650 to $2,500$ Ma, with a major unimodal peak of ~ 800 Ma grains.

5. Discussion

Data presented here support a tectonic model in which the oLH was emplaced during Miocene movement along the Tons thrust via in-sequence thrust propagation (Webb et al., 2011) (Figure 5). While it may be interpreted that cooling ages from the oLH presented here reflect exhumation-related cooling after initial emplacement, we interpret these ages to reflect exhumation linked to southward thrust advancement and displacement along the Tons thrust for several reasons. Unlike the vast majority of LH rocks across the orogen, which have been exhumed from great depths, including high-grade iLH rocks with peak temperatures of $\sim 600^\circ\text{C}$ (Caddick et al., 2007), rocks from the oLH were buried just deep enough to reset the ZHe system. The oLH lack published $^{40}\text{Ar}/^{39}\text{Ar}$ data, and Raman spectroscopy of carbonaceous material (RSCM thermometry) from the oLH near Mussoorie record peak metamorphic temperatures not exceeding 330°C (Celerier

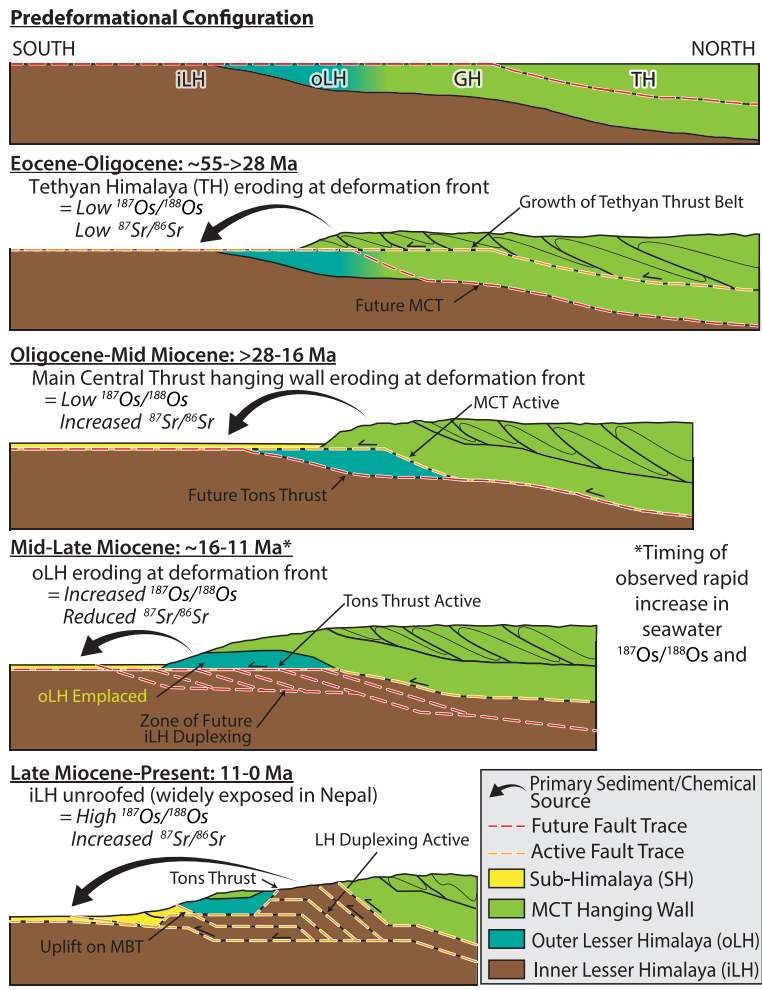


Figure 5. Schematic model of Himalayan thrust belt advance and exhumation. Current bedrock and foreland basin data suggest southward propagation of thrusting away from the MCT and in-sequence activation of the Tons thrust at ~16 Ma, resulting in a shift in exhumation from MCT hanging wall rocks enriched in $^{87}\text{Sr}/^{86}\text{Sr}$ to oLH rocks that are depleted in $^{87}\text{Sr}/^{86}\text{Sr}$ and enriched in $^{187}\text{Os}/^{188}\text{Os}$. iLH duplexing begins to develop at ~11 Ma and folds the Tons thrust to its modern day south-dipping orientation. As late Miocene iLH duplexing developed, the zone of exhumation began to shift northward and the iLH, which is relatively enriched in $^{187}\text{Os}/^{188}\text{Os}$, breached the surface. Exhumation along the MBT initiated by ~7 Ma. Modified after Yu et al. (2015).

et al., 2009a). Rocks from the oLH would, as a result, likely yield pre-Himalayan $^{40}\text{Ar}/^{39}\text{Ar}$ white mica ages. Therefore, the oLH was likely a source for the increased abundance of detrital white mica grains with pre-Himalayan $^{40}\text{Ar}/^{39}\text{Ar}$ ages observed in the foreland basin at ~17 Ma (Najman et al., 2009; White et al., 2002). Zircon fission track ages from oLH rocks structurally beneath the Lansdowne klippe also yielded pre-Himalayan cooling ages, indicating that these rocks were never buried to temperatures greater than 230–250°C (Yu, 2014). Thus, oLH rocks across NW India experienced peak temperatures of ~180° to 230°C, and ZHe cooling ages presented here provide the only available thermochronometric constraints for the onset of oLH exhumation. Given evidence that (1) oLH heating to relatively low peak temperatures (~180° to 230°C) was primarily the result of burial under the MCT sheet, (2) a major provenance shift occurred in the foreland basin at this time (Najman et al., 2009; White et al., 2002), and (3) activation of the Tons thrust was the result of in-sequence southward thrust propagation (Webb et al., 2011; Yu et al., 2015), we interpret oLH ZHe ages to have resulted from exhumation due to southward propagation of thrusting away from the MCT and to the Tons thrust at a minimum age of 16 Ma. We suggest that this initiated focused exhumation at a frontal ramp system linked to the basal décollement, in which oLH rocks likely crossed the advected

ZHe T_c isotherm at relatively high angles along more vertical particle pathways, likely resulting in rapid cooling.

Cooling ages from MCT hanging wall klippen provide useful constraints on the kinematic evolution of northwest India, as they are erosional remnants of rocks structurally emplaced above the LH and preserve cooling ages that reflect older exhumation of these rocks prior to the onset of oLH exhumation. This is best observed near Shimla where rocks from the Shimla MCT klippe preserve ZHe cooling ages between ~20–24 Ma structurally above oLH rocks, which preserve ZHe cooling ages of ~10–12 Ma that do not show a correlation with elevation (Figure 1). Samples from the Shimla and Lansdowne MCT klippen yielded ZHe ages ranging from ~20–23 Ma, and suggest that MCT hanging wall rocks were emplaced above the oLH before deformation propagated to the LH. Uniform ages produced from these MCT hanging wall klippen indicate relatively synchronous MCT exhumation along strike for over 200 km from Shimla to Lansdowne at this time until thrusting advanced southward and into the oLH. Once the LH began to accommodate deformation, exhumation-related cooling of deeply buried MCT hanging wall rocks to the north of the Tons thrust would likely have been driven by shortening within the iLH after initial MCT emplacement.

Lower grade, upper oLH rocks, including shallow marine Cretaceous–Paleogene deposits of the Singtali–Subathu Formations, are structurally beneath much higher grade MCT hanging wall rocks in Mussoorie and Lansdowne. This relationship is even more evident from detrital zircon U–Pb analyses from the Mussoorie syncline, where an abundance of Early Cretaceous grains is present only in Singtali–Subathu deposits, while the highly sheared MCT hanging wall sample (MGA01) from the Mussoorie klippe, collected less than ~30 meters above samples MGP01, yielded grains no younger than ~650 Ma, and a major peak of ~800 Ma grains (not observed in sample MGP01). The abundance of Neoproterozoic grains from the sheared Mussoorie MCT klippe suggests that these rocks are part of the succession that rests above the ~500 Myr regional unconformity seen across northern India and were thrust above the underlying Singtali–Subathu deposits. Within the Tons thrust footwall, sparse lenses of Singtali–Subathu deposits also lie unconformably above iLH strata (Valdiya, 1980; Webb et al., 2011) indicating that the iLH and oLH were likely in relatively close lateral proximity to each other along the passive margin of India before LH deformation. Uplifted Singtali–Subathu rocks also allow for stratigraphic constraints on the uppermost units exposed at the surface before deformation within the LH. In Mussoorie, Singtali–Subathu rocks lie unconformably above the Upper Tal Group and indicate the minimum total predeformational oLH thickness here to be ~3–4 km.

Uniform cooling ages of ~16 Ma from oLH and Singtali–Subathu rocks beneath the Lansdowne and Mussoorie MCT klippen indicate that these rocks were sufficiently buried below the ZHe closure window by MCT overburden prior to 16 Ma. Ages from the oLH decrease to the west to ~10–12 Ma where mostly Shimla Group rocks—the deepest rocks of the oLH located near the base of the Tons thrust sheet—are exposed. These ages, as well as primarily ~10 Ma iLH ZHe ages to the north, are likely due to exhumation relating to iLH duplex development, which folded the Tons thrust at depth and resulted in the present-day south-dipping fault plane (Figure 5). We postulate that Lesser Himalayan duplexing at this time drove a northward shift in exhumation that resulted in erosion of MCT hanging wall rocks and formation of iLH windows, much like the modern day Kullu–Rampur iLH window to the west (Figure 1). From ~11 Ma on, the majority of MCT hanging wall rocks above the LH have been removed, exposing much of the LH and leaving behind remnants of the MCT hanging wall now preserved as klippen. A single lower oLH Shimla Group sample, collected just north of the MBT and south of the MCT hanging wall klippen, produced an age of ~7 Ma, indicating cooling due to more recent exhumation along the MBT.

This study presents three lines of evidence for the onset of rapid exhumation of oLH strata containing ^{187}Os enriched black shale at ~16 Ma. The first line of evidence comes from ZHe data collected near Mussoorie, where the original Neoproterozoic–Cambrian oLH succession is largely preserved within the structural synform (Hughes et al., 2005; Jiang et al., 2002; Valdiya, 1980). Here uniform ZHe cooling ages of ~16 Ma exist within the entire ~3–4 km thick oLH stratigraphic package, on both sides of the synform, indicating that this package was likely rapidly exhumed at ~16 Ma (Figure 3). Second, ZHe data from the Mussoorie syncline show a strong age correlation with elevation where uniform ~16 Ma ZHe cooling ages were yielded across ~1.5 km relief (Figure 4b). These data are consistent with rapid exhumation, and indicate, at a first-order, a probable minimum exhumation rate of 1.5 km/Myr for these strata. This rate was calculated by excluding the younger Mussoorie ZHe cooling ages of ~11 Ma from the lowest exposed portion of the oLH and iLH north of the Tons thrust, which likely passed through the ZHe closer temperature during iLH

duplexing, and ~ 7 Ma from the Shimla Group sample collected farthest south (likely relating to exhumation corresponding to more recent uplift along the MBT). While data from multiple thermochronometric systems would greatly improve this rate estimate, oLH rocks sampled were not sufficiently heated to reset zircon fission track ages, and these rocks unfortunately did not yield quality apatite separates for lower temperature cooling ages. Lastly, strata from the 13–17 Ma upper Dharamsala foreland basin deposits preserve a record of the tectonic and exhumational evolution of the hinterland at this time, and show a distinct shift from dominantly metamorphic source rocks to lower-grade sedimentary sources (Najman, 2006; Najman et al., 2009; White et al., 2001, 2002). The abundance of 16–17 Ma ZHe cooling ages, and very short depositional lag times of 0–3 Myr, clearly demonstrates that Himalayan source rocks, likely sourced from the oLH Krol–Tal belt and MCT hanging wall rocks, were rapidly exhumed and eroded into the foreland basin at this time (Figure 4).

Collectively, these data provide strong support for the hypothesis that Himalayan tectonic unroofing and bedrock weathering drove Neogene seawater $^{87}\text{Sr}/^{86}\text{Sr}$ and $^{187}\text{Os}/^{188}\text{Os}$ variation. The shifts in weathering substrates were highly dependent on the tectonic and kinematic evolution of the thrust belt, and our data indicate a southward advancement in thrusting into the MCT footwall at ~ 16 Ma in northwest India, in agreement with provenance shifts previously observed in the foreland basin at this time (Najman, 2006; Najman et al., 2009; White et al., 2002). Thrust advancement around this time is further evinced by thermochronometric data in western India (Deeken et al., 2011), Nepal (Bernet et al., 2006), and Bhutan (Long et al., 2012) which, in conjunction with our new data, supports the potential for an orogen-wide pulse of LH exhumation at the front of the thrust system due to a major reorganization of the orogenic wedge. Strata enriched in ^{187}Os within the Tons thrust hanging wall may have spanned the length of the orogen, but were removed across Nepal due to erosion since initial unroofing at 16 Ma, with the strata preserved in the oLH being a regional remnant of this once-extensive belt of material (Myrow et al., 2015; Yu et al., 2015). However, this study only provides evidence for unroofing of oLH strata in northwest India at ~ 16 Ma, and more focused detrital studies on age equivalent foreland basin strata across the entire orogeny must be done to corroborate this interpretation. For this reason, the volume of total oLH material eroded remains speculative. Regardless of whether this material spanned the entire orogen or not, simple box modeling suggests that with a minimum exhumation rate of at least ~ 1.5 km/Myr (consistent with data presented here), the minimum volume of eroded oLH bedrock, constrained by the total present day areal extent of the oLH and minimal thickness of Os enriched oLH strata, is significant enough to account for at least half of the observed $^{187}\text{Os}/^{188}\text{Os}_{(\text{sw})}$ increase between 16 and 11 Ma (Myrow et al., 2015). We refer the reader to the supporting information of Myrow et al. (2015) for details of this mixing model, which incorporates an average oLH $^{187}\text{Os}/^{188}\text{Os}$ value of 3.0 as a primary source from 16 to 11 Ma, and average iLH $^{187}\text{Os}/^{188}\text{Os}$ value of 7.8 as the primary source from 11 Ma to 1 Ma.

The unroofing of ^{187}Os enriched oLH strata at ~ 16 Ma likely initiated the increase in $^{187}\text{Os}/^{188}\text{Os}_{(\text{sw})}$ and a coeval decrease in slope in $^{87}\text{Sr}/^{86}\text{Sr}_{(\text{sw})}$ due to exhumation of stratigraphically thick Krol Group carbonates, which are relatively less radiogenic than MCT hanging wall rocks (Myrow et al., 2015) (Figures 4a and 5). Our thermochronologic data indicate that LH duplex development by ~ 11 Ma shifted the zone of focused exhumation north of the Tons thrust, exhuming MCT hanging wall rock until iLH rocks breached the surface. However, direct timing constraints on iLH exposure in northwest India are lacking, and can only be constrained with these data to a maximum age of ~ 11 Ma. Cooling ages presented here from the Paleoproterozoic iLH are in agreement with the reported ~ 11 Ma unroofing of Paleo-Mesoproterozoic LH rocks in Nepal (Chesley et al., 2000; DeCelles et al., 1998, 2000) and northwest India (Caddick et al., 2007). Once unroofed, older iLH strata enriched in radiogenic ^{187}Os continued to facilitate the ongoing increase in $^{187}\text{Os}/^{188}\text{Os}_{(\text{sw})}$ as oLH strata eroded away across the orogen. Paleoproterozoic LH strata and high-grade rocks of the Muniari Group are significantly enriched in radiogenic Sr (Ahmad et al., 2000; Bickle et al., 2001), and the unroofing of these rocks could explain a minor rate increase in $^{87}\text{Sr}/^{86}\text{Sr}_{(\text{sw})}$ reported during the Late Miocene to the present (Derry & France-Lanord, 1996).

6. Conclusions

The relationship between weathering of distinct Himalayan source rocks and observed global shifts in the $^{87}\text{Sr}/^{86}\text{Sr}$ and $^{187}\text{Os}/^{188}\text{Os}$ seawater records is critical because these records have been utilized to various

degrees to track shifts in global silicate and black shale weathering as a means to reconstruct long-term carbon cycling. Cenozoic $^{87}\text{Sr}/^{86}\text{Sr}_{(\text{sw})}$ and $^{187}\text{Os}/^{188}\text{Os}_{(\text{sw})}$ records appear to have been strongly influenced by the weathering and erosion of isotopically distinct Himalayan rocks exposed at the surface, which is primarily controlled by spatiotemporal kinematic and climatic shifts within the Himalayan thrust belt. If correct, this would indicate a rapid seawater response to tectonically driven chemical input. Seawater isotopic records could thus have been largely driven by the composition of weathering substrates, and these source-driven changes would have been independent of changes in the extent of global weathering. Given the propensity for regional bedrock influences, seawater Sr and Os isotopic records should not be considered reliable proxies for tracking deep-time silicate or oxidative sulfide weathering. Thus, utilization of these records to develop a mechanistic understanding of the factors controlling atmospheric CO_2 levels throughout Earth history remains problematic.

Acknowledgments

This work has been supported by an NSF-Tectonics grant to NRM, DFS, and BKH (EAR-1450976); NSF-Sedimentary Geology and Paleobiology grants to NCH (EAR-1124303) and to PMM (EAR-1124518); the Yale University Flint Postdoctoral Fellowship to NRM; and an ExxonMobil Geological Society Graduate Research Grant to CLC. M. Brandon and D. Evans provided valuable discussions. We thank two anonymous reviewers for their thorough and constructive comments that improved the clarity of this manuscript. We gratefully acknowledge critical reviews by A.C. Pierson-Wickmann, L. Derry, P. DeCelles, and an anonymous reviewer on an earlier version of this manuscript. All data presented here are available in the supporting information.

References

- Ahmad, T., Harris, N., Bickle, M., Chapman, H., Bunbury, J., & Prince, C. (2000). Isotopic constraints on the structural relationships between the Lesser Himalayan Series and the High Himalayan Crystalline Series, Garhwal Himalaya. *Geological Society of America Bulletin*, *112*(3), 467–477.
- Auden, J. B. (1934). The geology of the Krol Belt. *Geological Survey of India Records*, *67*, 357–454.
- Bataille, C. P., Willis, A., Yang, X., & Liu, X. M. (2017). Continental igneous rock composition: A major control of past global chemical weathering. *Science Advances*, *3*(3), e1602183.
- Berner, R. A., Lasaga, A. C., & Garrels, R. M. (1983). The carbonate-silicate geochemical cycle and its effect on atmospheric carbon-dioxide over the past 100 million years. *American Journal of Science*, *283*(7), 641–683.
- Bernet, M., van der Beek, P., Pik, R., Huyghe, P., Mugnier, J. L., Labrin, E., & Szulc, A. (2006). Miocene to recent exhumation of the central Himalaya determined from combined detrital zircon fission-track and U/Pb analysis of Siwalik sediments, western Nepal. *Basin Research*, *18*(4), 393–412.
- Bickle, M. J., Harris, N. B. W., Bunbury, J. M., Chapman, H. J., Fairchild, I. J., & Ahmad, T. (2001). Controls on the Sr-87/Sr-86 ratio of carbonates in the Garhwal Himalaya, headwaters of the Ganges. *Journal of Geology*, *109*(6), 737–753.
- Bickle, M. J., Tipper, E. D., Galy, A., Chapman, H., & Harris, N. (2015). On discrimination between carbonate and silicate inputs to Himalayan rivers. *American Journal of Science*, *315*(2), 120–166.
- Blum, J. D., Gazis, C. A., Jacobson, A. D., & Page Chamberlain, C. (1998). Carbonate versus silicate weathering in the Raikhot watershed within the High Himalayan Crystalline Series. *Geology*, *26*(5), 411–414.
- Caddick, M. J., Bickle, M. J., Harris, N. B. W., Holland, T. J. B., Horstwood, M. S. A., Parrish, R. R., & Ahmad, T. (2007). Burial and exhumation history of a Lesser Himalayan schist: Recording the formation of an inverted metamorphic sequence in NW India. *Earth and Planetary Science Letters*, *264*(3–4), 375–390.
- Celerier, J., Harrison, T. M., Beyssac, O., Herman, F., Dunlap, W. J., & Webb, A. A. G. (2009a). The Kumaun and Garhwal Lesser Himalaya, India: Part 2. Thermal and deformation histories. *Geological Society of America Bulletin*, *121*(9–10), 1281–1297.
- Celerier, J., Harrison, T. M., Webb, A. A. G., & Yin, A. (2009b). The Kumaun and Garhwal Lesser Himalaya, India: Part 1. Structure and stratigraphy. *Geological Society of America Bulletin*, *121*(9–10), 1262–1280.
- Chambers, J., Caddick, M., Argles, T., Horstwood, M., Sherlock, S., Harris, N., et al. (2009). Empirical constraints on extrusion mechanisms from the upper margin of an exhumed high-grade orogenic core, Sutlej valley, NW India. *Tectonophysics*, *477*(1–2), 77–92.
- Chesley, J. T., Quade, J., & Ruiz, J. (2000). The Os and Sr isotopic record of Himalayan paleorivers: Himalayan tectonics and influence on ocean chemistry. *Earth and Planetary Science Letters*, *179*(1), 115–124.
- Cox, G. M., Halverson, G. P., Stevenson, R. K., Vokaty, M., Poirier, A., Kunzmann, M., et al. (2016). Continental flood basalt weathering as a trigger for Neoproterozoic Snowball Earth. *Earth and Planetary Science Letters*, *446*, 89–99.
- DeCelles, P. G., Carrapa, B., Gehrels, G. E., Chakraborty, T., & Ghosh, P. (2016). Along-strike continuity of structure, stratigraphy, and kinematic history in the Himalayan thrust belt: The view from Northeastern India. *Tectonics*, *35*, 2995–3027. <https://doi.org/10.1002/2016TC004298>
- DeCelles, P. G., Gehrels, G. E., Quade, J., LaReau, B., & Spurlin, M. (2000). Tectonic implications of U-Pb zircon ages of the Himalayan orogenic belt in Nepal. *Science*, *288*(5465), 497–499.
- DeCelles, P. G., Gehrels, G. E., Quade, J., Ojha, T. P., Kapp, P. A., & Upreti, B. N. (1998). Neogene foreland basin deposits, erosional unroofing, and the kinematic history of the Himalayan fold-thrust belt, western Nepal. *Geological Society of America Bulletin*, *110*(1), 2–21.
- DeCelles, P. G., Robinson, D. M., Quade, J., Ojha, T. P., Garzzone, C. N., Copeland, P., & Upreti, B. N. (2001). Stratigraphy, structure, and tectonic evolution of the Himalayan fold-thrust belt in western Nepal. *Tectonics*, *20*(4), 487–509.
- Deeken, A., Thiede, R. C., Sobel, E. R., Hourigan, J. K., & Strecker, M. R. (2011). Exhumational variability within the Himalaya of northwest India. *Earth and Planetary Science Letters*, *305*(1–2), 103–114.
- Derry, L. A., & France-Lanord, C. (1996). Neogene Himalayan weathering history and river Sr-87/Sr-86: Impact on the marine Sr record. *Earth and Planetary Science Letters*, *142*(1–2), 59–74.
- Dodson, M. H. (1973). Closure temperature in cooling geochronological and petrological systems. *Contributions to Mineralogy and Petrology*, *40*(3), 259–274.
- Edmond, J. M. (1992). Himalayan tectonics, weathering processes, and the strontium isotope record in marine limestones. *Science*, *258*(5088), 1594–1597.
- English, N. B., Quade, J., DeCelles, P. G., & Garzzone, C. N. (2000). Geologic control of Sr and major element chemistry in Himalayan Rivers, Nepal. *Geochimica et Cosmochimica Acta*, *64*(15), 2549–2566.
- Farley, K. A., Wolf, R. A., & Silver, L. T. (1996). The effects of long alpha-stopping distances on (U-Th)/He ages. *Geochimica et Cosmochimica Acta*, *60*(21), 4223–4229.
- Feng, R., Machado, N., & Ludden, J. (1993). Lead geochronology of zircon by laserprobe-inductively coupled plasma-mass spectrometry (Lp-lcpms). *Geochimica et Cosmochimica Acta*, *57*(14), 3479–3486.
- France-Lanord, C., Derry, L., & Michard, A. (1993). Evolution of the Himalaya since Miocene time: Isotopic and sedimentological evidence from the Bengal Fan. *Geological Society Special Publications*, *74*(1), 603–621.

- Fryer, B. J., Jackson, S. E., & Longerich, H. P. (1993). The application of laser-ablation microprobe-inductively coupled plasma-mass spectrometry (Lam-Icp-MS) to in-situ (U)-Pb geochronology. *Chemical Geology*, 109(1–4), 1–8.
- Galy, A., France-Lanord, C., & Derry, L. A. (1999). The strontium isotopic budget of Himalayan rivers in Nepal and Bangladesh. *Geochimica et Cosmochimica Acta*, 63(13–14), 1905–1925.
- Georg, R. B., West, A. J., Vance, D., Newman, K., & Halliday, A. N. (2013). Is the marine osmium isotope record a probe for CO₂ release from sedimentary rocks? *Earth and Planetary Science Letters*, 367, 28–38.
- Goddéris, Y., Le Hir, G., Macouin, M., Donnadieu, Y., Hubert-Théou, L., Dera, G., et al. (2017). Paleogeographic forcing of the strontium isotopic cycle in the Neoproterozoic. *Gondwana Research*, 42, 151–162.
- Guenther, W. R., Reiners, P. W., Ketcham, R. A., Nasdala, L., & Giester, G. (2013). Helium diffusion in natural zircon: Radiation damage, anisotropy, and the interpretation of zircon (U-Th)/He thermochronology. *American Journal of Science*, 313(3), 145–198.
- Harris, N. (1995). Significance of Weathering Himalayan Metasedimentary Rocks and leucogranites for the Sr isotope evolution of seawater during the early Miocene. *Geology*, 23(9), 795–798.
- Harris, N., Bickle, M., Chapman, H., Fairchild, I., & Bunbury, J. (1998). The significance of Himalayan rivers for silicate weathering rates: Evidence from the Bhoté Kosi tributary. *Chemical Geology*, 144(3–4), 205–220.
- Hodell, D. A., Mueller, P. A., & Garrido, J. R. (1991). Variations in the strontium isotopic composition of seawater during the Neogene. *Geology*, 19(1), 24–27.
- Hughes, N. C. (2016). The Cambrian palaeontological record of the Indian subcontinent. *Earth-Science Reviews*, 159, 428–461.
- Hughes, N. C., Peng, S. C., Bhargava, O. N., Ahluwalia, A. D., Walia, S., Myrow, P. M., & Parcha, S. K. (2005). Cambrian biostratigraphy of the Tal Group, Lesser Himalaya, India, and early Tsanglangpuan (late early Cambrian) trilobites from the Nigali Dhar syncline. *Geological Magazine*, 142(1), 57–80.
- Jiang, G., Christie-Blick, N., Kaufman, A. J., Banerjee, D. M., & Rai, V. (2003). Carbonate platform growth and cyclicity at a terminal Proterozoic passive margin, Infra Krol Formation and Krol Group, Lesser Himalaya, India. *Sedimentology*, 50(5), 921–952.
- Jiang, G. Q., Christie-Blick, N., Kaufman, A. J., Banerjee, D. M., & Rai, V. (2002). Sequence stratigraphy of the neoproterozoic Infra Krol Formation and Krol Group, Lesser Himalaya, India. *Journal of Sedimentary Research*, 72(4), 524–542.
- Kump, L. R., Brantley, S. L., & Arthur, M. A. (2000). Chemical, weathering, atmospheric CO₂, and climate. *Annual Review of Earth and Planetary Sciences*, 28(1), 611–667.
- Long, S. P., McQuarrie, N., Tobgay, T., Coutand, I., Cooper, F. J., Reiners, P. W., et al. (2012). Variable shortening rates in the eastern Himalayan thrust belt, Bhutan: Insights from multiple thermochronologic and geochronologic data sets tied to kinematic reconstructions. *Tectonics*, 31, TC5004. <https://doi.org/10.1029/2012TC003155>
- Mandal, S., Robinson, D. M., Khanal, S., & Das, O. (2015). Redefining the tectonostratigraphic and structural architecture of the Almorá klippe and the Ramgarh–Munsiari thrust sheet in NW India. *Geological Society Special Publications*, 412(1), 247–269.
- Mandal, S., Robinson, D. M., Kohn, M. J., Khanal, S., Das, O., & Bose, S. (2016). Zircon U-Pb ages and Hf isotopes of the Askot klippe, Kumaun, northwest India: Implications for Paleoproterozoic tectonics, basin evolution and associated metallogeny of the northern Indian cratonic margin. *Tectonics*, 35, 965–982. <https://doi.org/10.1002/2015TC004064>
- McKenzie, N. R., Hughes, N. C., Myrow, P. M., Xiao, S. H., & Sharma, M. (2011). Correlation of Precambrian-Cambrian sedimentary successions across northern India and the utility of isotopic signatures of Himalayan lithotectonic zones. *Earth and Planetary Science Letters*, 312(3–4), 471–483.
- McQuarrie, N., Robinson, D., Long, S., Tobgay, T., Grujic, D., Gehrels, G., & Ducea, M. (2008). Preliminary stratigraphic and structural architecture of Bhutan: Implications for the along strike architecture of the Himalayan system. *Earth and Planetary Science Letters*, 272(1–2), 105–117.
- Misra, S., & Froelich, P. N. (2012). Lithium isotope history of cenozoic seawater: Changes in silicate weathering and reverse weathering. *Science*, 335(6070), 818–823.
- Myrow, P. M., Hughes, N. C., Derry, L. A., McKenzie, N. R., Jiang, G. Q., Webb, A. A. G., et al. (2015). Neogene marine isotopic evolution and the erosion of Lesser Himalayan strata: Implications for Cenozoic tectonic history. *Earth and Planetary Science Letters*, 417, 142–150.
- Myrow, P. M., Hughes, N. C., Goodge, J. W., Fanning, C. M., Williams, I. S., Peng, S. C., et al. (2010). Extraordinary transport and mixing of sediment across Himalayan central Gondwana during the Cambrian-Ordovician. *Geological Society of America Bulletin*, 122(9–10), 1660–1670.
- Myrow, P. M., Hughes, N. C., Paulsen, T. S., Williams, I. S., Parcha, S. K., Thompson, K. R., et al. (2003). Integrated tectonostratigraphic analysis of the Himalaya and implications for its tectonic reconstruction. *Earth and Planetary Science Letters*, v. 212(3–4), 433–441.
- Najman, Y. (2006). The detrital record of orogenesis: A review of approaches and techniques used in the Himalayan sedimentary basins. *Earth-Science Reviews*, 74(1–2), 1–72.
- Najman, Y., Bickle, M., Garzanti, E., Pringle, M., Barfod, D., Brozovic, N., . . . Ando, S. (2009). Reconstructing the exhumation history of the Lesser Himalaya, NW India, from a multitechnique provenance study of the foreland basin Siwalik Group. *Tectonics*, 28, TC5018. <https://doi.org/10.1029/2009TC002506>
- Palmer, M. R., & Edmond, J. M. (1989). The strontium isotope budget of the modern ocean. *Earth and Planetary Science Letters*, 92(1), 11–26.
- Paton, C., Hellstrom, J., Paul, B., Woodhead, J., & Hergt, J. (2011). Iolite: Freeware for the visualisation and processing of mass spectrometric data. *Journal of Analytical Atomic Spectrometry*, 26(12), 2508–2518.
- Pegram, W. J., Krishnaswami, S., Ravizza, G. E., & Turekian, K. K. (1992). The record of sea-water Os-187/Os-186 variation through the Cenozoic. *Earth and Planetary Science Letters*, 113(4), 569–576.
- Petrus, J. A., & Kamber, B. S. (2012). VizualAge: A novel approach to laser ablation ICP-MS U-Pb geochronology data reduction. *Geostandards and Geoanalytical Research*, 36(3), 247–270.
- Peucker-Ehrenbrink, B., & Ravizza, G. (2000). The marine osmium isotope record. *Terra Nova*, 12(5), 205–219.
- Pierson-Wickmann, A. C., Reisberg, L., & France-Lanord, C. (2000). The Os isotopic composition of Himalayan river bedloads and bedrocks: Importance of black shales. *Earth and Planetary Science Letters*, 176(2), 203–218.
- Pierson-Wickmann, A.-C., Reisberg, L., & France-Lanord, C. (2002). Impure marbles of the Lesser Himalaya: Another source of continental radiogenic osmium. *Earth and Planetary Science Letters*, v. 204(1–2), 203–214.
- Quade, J., English, N., & DeCelles, P. G. (2003). Silicate versus carbonate weathering in the Himalaya: A comparison of the Arun and Seti River watersheds. *Chemical Geology*, 202(3–4), 275–296.
- Quade, J., Roe, L., DeCelles, P. G., & Ojha, T. P. (1997). The late Neogene Sr-87/Sr-86 record of lowland Himalayan rivers. *Science*, 276(5320), 1828–1831.
- Ravizza, G. (1993). Variations of the 187Os/186Os ratio of seawater over the past 28 million years as inferred from metalliferous carbonates. *Earth and Planetary Science Letters*, 118(1), 335–348.
- Raymo, M. E., & Ruddiman, W. F. (1992). Tectonic forcing of late Cenozoic climate. *Nature*, 359(6391), 117–122.

- Reiners, P. W., & Brandon, M. T. (2006). Using thermochronology to understand orogenic erosion. *Annual Review of Earth and Planetary Sciences*, 34(1), 419–466.
- Reiners, P. W., Farley, K. A., & Hickey, H. J. (2002). He diffusion and (U-Th)/He thermochronometry of zircon: Initial results from Fish Canyon Tuff and Gold Butte. *Tectonophysics*, 349(1–4), 297–308.
- Reiners, P. W., Spell, T. L., Nicolescu, S., & Zanetti, K. A. (2004). Zircon (U-Th)/He thermochronometry: He diffusion and comparisons with ⁴⁰Ar/³⁹Ar dating. *Geochimica et Cosmochimica Acta*, 68(8), 1857–1887.
- Richards, A., Argles, T., Harris, N., Parrish, R., Ahmad, T., Darbyshire, F., & Draganits, E. (2005). Himalayan architecture constrained by isotopic tracers from clastic sediments. *Earth and Planetary Science Letters*, 236(3–4), 773–796.
- Robinson, D. M., DeCelles, P. G., Garzzone, C. N., Pearson, O. N., Harrison, T. M., & Catlos, E. J. (2003). Kinematic model for the Main Central thrust in Nepal. *Geology*, 31(4), 359–362.
- Robinson, D. M., & Martin, A. J. (2014). Reconstructing the Greater Indian margin: A balanced cross section in central Nepal focusing on the Lesser Himalayan duplex. *Tectonics*, 33, 2143–2168. <https://doi.org/10.1002/2014TC003564>
- Robinson, D. M., & Pearson, O. N. (2013). Was Himalayan normal faulting triggered by initiation of the Ramgarh-Munsiari thrust and development of the Lesser Himalayan duplex? *International Journal of Earth Sciences*, 102(7), 1773–1790.
- Ruiz, G. M. H., Seward, D., & Winkler, W. (2004). Detrital thermochronology - a new perspective on hinterland tectonics, an example from the Andean Amazon Basin, Ecuador. *Basin Research*, v, 16(3), 413–430.
- Sarin, M. M., Krishnaswami, S., Dilli, K., Somayajulu, B. L. K., & Moore, W. S. (1989). Major Ion Chemistry of the Ganga-Brahmaputra River System - Weathering Processes and Fluxes to the Bay of Bengal. *Geochimica et Cosmochimica Acta*, 53(5), 997–1009.
- Singh, S. K., Trivedi, J. R., & Krishnaswami, S. (1999). Re-Os isotope systematics in black shales from the Lesser Himalaya: Their chronology and role in the Os-187/Os-188 evolution of seawater. *Geochimica et Cosmochimica Acta*, 63(16), 2381–2392.
- Singh, S. K., Trivedi, J. R., Pande, K., Ramesh, R., & Krishnaswami, S. (1998). Chemical and strontium, oxygen, and carbon isotopic compositions of carbonates from the Lesser Himalaya: Implications to the strontium isotope composition of the source waters of the Ganga, Ghaghara, and the Indus rivers. *Geochimica et Cosmochimica Acta*, v, 62(5), 743–755.
- Thiede, R. C., Bookhagen, B., Arrowsmith, J. R., Sobel, E. R., & Strecker, M. R. (2004). Climatic control on rapid exhumation along the Southern Himalayan Front. *Earth and Planetary Science Letters*, 222(3–4), 791–806.
- Torres, M. A., West, A. J., & Li, G. J. (2014). Sulphide oxidation and carbonate dissolution as a source of CO₂ over geological timescales. *Nature*, 507(7492), 346–349.
- Valdiya, K. S. (1980). *Geology of Kumaun Lesser Himalaya* (291 p.). Dehra Dun, India: Wadia Institute of Himalayan Geology.
- Vannay, J. C., Grasmann, B., Rahn, M., Frank, W., Carter, A., Baudraz, V., & Cosca, M. (2004). Miocene to Holocene exhumation of metamorphic crustal wedges in the NW Himalaya: Evidence for tectonic extrusion coupled to fluvial erosion. *Tectonics*, 23, TC1014. <https://doi.org/10.1029/2002TC001429>
- Veizer, J. (1989). Strontium isotopes in seawater through time. *Annual Review of Earth and Planetary Sciences*, 17(1), 141–167.
- Veizer, J., Ala, D., Azmy, K., Bruckschen, P., Buhl, D., Bruhn, F., et al. (1999). ⁸⁷Sr/⁸⁶Sr, $\delta^{13}\text{C}$ and $\delta^{18}\text{O}$ evolution of Phanerozoic seawater. *Chemical Geology*, 161(1), 59–88.
- Vermeesch, P. (2004). How many grains are needed for a provenance study? *Earth and Planetary Science Letters*, 224(3–4), 441–451.
- Webb, A. A. G. (2013). Preliminary balanced palinspastic reconstruction of Cenozoic deformation across the Himachal Himalaya (northwestern India). *Geosphere*, 9(3), 572–587.
- Webb, A. A. G., Yin, A., Harrison, T. M., Celerier, J., Gehrels, G. E., Manning, C. E., & Grove, M. (2011). Cenozoic tectonic history of the Himachal Himalaya (northwestern India) and its constraints on the formation mechanism of the Himalayan orogen. *Geosphere*, 7(4), 1013–1061.
- West, A. J., Bickle, M. J., Collins, R., & Brasington, J. (2002). Small-catchment perspective on Himalayan weathering fluxes. *Geology*, 30(4), 355–358.
- White, N. M., Parrish, R. R., Bickle, M. J., Najman, Y. M. R., Burbank, D., & Maithani, A. (2001). Metamorphism and exhumation of the NW Himalaya constrained by U-Th-Pb analyses of detrital monazite grains from early foreland basin sediments. *Journal of the Geological Society*, 158(4), 625–635.
- White, N. M., Pringle, M., Garzanti, E., Bickle, M., Najman, Y., Chapman, H., & Friend, P. (2002). Constraints on the exhumation and erosion of the High Himalayan Slab, NW India, from foreland basin deposits. *Earth and Planetary Science Letters*, 195(1–2), 29–44.
- Wolfe, M. R., & Stockli, D. F. (2010). Zircon (U-Th)/He thermochronometry in the KTB drill hole, Germany, and its implications for bulk He diffusion kinetics in zircon. *Earth and Planetary Science Letters*, 295(1–2), 69–82.
- Yin, A. (2006). Cenozoic tectonic evolution of the Himalayan orogen as constrained by along-strike variation of structural geometry, exhumation history, and foreland sedimentation. *Earth-Science Reviews*, 76(2), 1–1–131.
- Yu, H. (2014). *Contractional tectonics: Investigations of ongoing construction of the Himalaya Fold-thrust Belt and the trishear model of fault-propagation folding* (Doctoral dissertation). LSU.
- Yu, H. J., Webb, A. A. G., & He, D. (2015). Extrusion vs. duplexing models of Himalayan mountain building 1: Discovery of the Pabbar thrust confirms duplex-dominated growth of the northwestern Indian Himalaya since Mid-Miocene. *Tectonics*, 34, 313–333. <https://doi.org/10.1002/2014TC003589>
- Zeitler, P. K., Herczeg, A. L., McDougall, I., & Honda, M. (1987). U-Th-He dating of apatite - a potential thermochronometer. *Geochimica et Cosmochimica Acta*, 51(10), 2865–2868.